Hot plastic deformation of aluminium alloy 2009–15%SiC_w composite

R. Kaibyshev, V. Kazyhanov, and F. Musin

The hot deformation behaviour of the discontinuously reinforced metal matrix composite aluminium alloy 2009(Al–3·8 wt-%Cu–1·3 wt-%Mg)–15 vol.-%SiC_w, produced via powder metallurgy, was studied by compression testing in the strain rate range 10^{-4}–10^{1} s^{-1} at temperatures ranging from 450 to 525°C. It was shown that the composite exhibits superplasticlike behaviour, which can be explained in terms of a threshold stress. This approach allowed calculation of the true activation energy and true values of the stress exponent. A strong temperature dependence of the threshold stresses was determined. Optical metallographic studies and TEM investigations were carried out to examine microstructural evolution. It was shown that superplastic deformation does not lead to the formation of a new macrostructure. Under superplastic conditions the SiC whiskers retain their orientation, while at both lower and higher strain rates the reinforcements rotate during deformation. As a result, superplastic deformation yields increased service properties. The origin of this phenomenon is discussed. MST/4998

The authors are at the Institute of Metals Superplasticity Problems RAS, Khalturina 39, Ufa, 450001, Russia (rustam@anrb.ru).
Manuscript received 19 February 2001; accepted 11 July 2001.

Introduction

Discontinuously reinforced metal matrix composites (MMCs) based on aluminium alloys exhibit a unique combination of high specific modulus and strength at room temperature.[1,2] This type of composite is characterised by a considerable formability. Secondary fabrication to manufacture parts from MMCs can involve conventional metal working such as extrusion, forging, or rolling technology. However, these MMCs exhibit low hot workability in comparison with monolithic aluminium alloys[2,3] owing to higher flow stresses and poor plasticity, which lead to surface breakup or cracking during the forging operation. This limits industrial application of the wrought MMCs.

Superplastic deformation is a unique, effective route for increasing the hot workability of MMCs.[3,4] Various studies have demonstrated that in discontinuously reinforced MMCs superplasticity is evident at high strain rates[3] ($\dot{\varepsilon} \geqslant 10^{-2}$ s^{-1}), whereas in bulk aluminium alloys optimum superplasticity is observed at lower strain rates[4,5] ($\dot{\varepsilon} \leqslant 10^{-3}$ s^{-1}). The phenomenon termed high strain rate superplasticity (HSRS) has been found in a number of different MMCs.[3,4] Although numerous studies have dealt with the mechanical behaviour of MMCs, experimental data relating to structural evolution are few, and the effect of superplastic deformation on the service properties of composites has not yet been reported. It is well known[1,2,6,7] that service properties of MMCs are closely related to the dominant whisker orientation. However, the effect of HSRS on alignment and redistribution of the reinforcements is unclear. It is also known[6–11] that elongated ceramic reinforcing elements have a tendency to rotate during plastic deformation, and to align themselves in the working direction.

Thus, in the present work, the deformation behaviour and microstructural evolution of 2009Al–15%SiC_w composite has been investigated. This composite is an advanced material used for aircraft wheels owing to its high strength and fatigue resistance as well as perfect superior capacity. Hot working parameters were examined using hot working simulators. All forging processes comprise basically the compressive deformation of a workpiece, and an axial compression test was chosen as the best candidate for this role. Specific attention has been paid to the effect of HSRS on the arrangement of the reinforcing elements and service properties of the 2009Al–15%SiC_w composite. The data obtained have been compared with data from tensile testing,[12,13] allowing estimation of the influence of the deformation method on HSRS in MMCs.

Experimental procedure

The composite 2009Al–15%SiC_w was produced via powder metallurgy from standard aluminium alloy 2009 and 15 vol.-%SiC whiskers. Composition of the matrix alloy was Al–3·8Cu–1·3Mg–0·25Si (wt-%).

Cylindrical specimens 10 mm in diameter and 13 mm in height were machined from hot rolled plate, with a thickness of 34 mm, produced by the Rockwell proprietary process.[13] The compression axis of the specimens coincided with the initial rolling direction. Compression tests were carried out at temperatures 450–525°C and strain rates from 10^{-4} to 10^{1} s^{-1} on a Schenck RMS-100 universal testing machine. A hydraulic machine, Schenck PSA-100A, was used for testing in the strain rate interval 10^{-1}–10^{1} s^{-1}. A graphite colloid in oil was used as high temperature lubricant. The specimens were cooled in air immediately after plastic deformation.

Values of the stress exponent n in the power law equation

$$\dot{\varepsilon} = A\sigma^{n} \exp(-Q/RT) \quad . \quad . \quad . \quad . \quad . \quad . \quad . \quad . \quad . \quad . \quad (1)$$

where R is the universal gas constant, A is a material constant, T is the temperature, and Q is the true activation energy, were defined from the slope of $\log\dot{\varepsilon}$ *v.* $\log\sigma$. The steady state stress σ and initial strain rate $\dot{\varepsilon}$, were used for these calculations. Values of the strain rate sensitivity

$$m = \partial(\log \sigma)/\partial(\log \dot{\varepsilon}) \quad . \quad . \quad . \quad . \quad . \quad . \quad . \quad . \quad . \quad . \quad (2)$$

were calculated as $m = 1/n$.

For examination of service properties the specimens were upset at $T = 500$°C and $\dot{\varepsilon} = 10^{-2}$ s^{-1} up to strain $\varepsilon = 70\%$. The compression axis matched the prior rolling direction. Specimens for evaluation of mechanical properties were cut along the compression axis, and examined using an Instron type machine at ambient temperature. Tension tests were carried out on smooth cylindrical specimens with a diameter of 5 mm and gauge section of 25 mm.

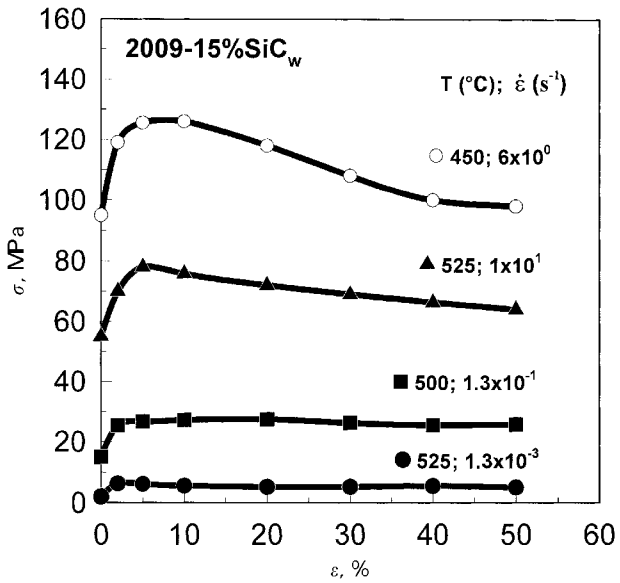

1 Typical true stress–strain curves for 2009Al–15%SiC$_w$ composite: at T=525°C, $\dot{\varepsilon}=1{\cdot}3\times10^{-3}$ s^{-1} and T=500°C, $\dot{\varepsilon}=1{\cdot}3\times10^{-1}$ s^{-1} σ–ε curves exhibit steady state flow, and at T=525°C, $\dot{\varepsilon}=1\times10^{1}$ s^{-1} and T=450°C, $\dot{\varepsilon}=6$ s^{-1}, the well developed heat stress can be recognised

The toughness and fracture strength were evaluated by static bending of specimens (7·5×7·5×55 mm) with a 1 mm U type lateral notch. Fracture toughness was determined as $K_{CU}=a_t/F$, where a_t is the total work of a specimen at failure estimated from a load–strain curve and F is the initial cross-sectional area of the specimen.[14] Fracture strength was calculated as the ratio of maximum load, taken from the above mentioned curve, to initial cross-sectional area of the specimen.

Metallographic analysis of deformed specimens was done using a Neophot-32 optical microscope, a JSM-840 scanning electron microscope, and an Epiquant structural analyser. Microstructural observations were carried out on specimens compressed up to a strain of 50% as well as composite in the as received condition. Specimens for optical microscopy were prepared from a section containing the compression axis by mechanical polishing and subsequent etching in Keller aqueous solution of 0·5%HF, 1·8%HCl, and 2·7%HNO_3. The fine structure was examined in a JEM-2000EX electron microscope using thin foils jet polished to perforation with a 20% nitric acid solution in methanol at −30°C and 15 V. Lattice dislocation density was determined from the number of dislocation intersections on the foil surface.[15] Grain boundary dislocation density was caculated as the ratio of number of dislocations/grain boundary length.[16]

Results

MECHANICAL BEHAVIOUR

Stress–strain curves

Typical true stress–strain curves for the 2009Al–15%SiC$_w$ composite are shown in Fig. 1. Two types of σ–ε curve can be distinguished. One type exhibits steady state flow after $\varepsilon\approx3\%$, at $\dot{\varepsilon}\leqslant10^{-2}$ s^{-1}. The other type of σ–ε curve is found at higher strain rates, and contains a well defined stress peak. Steady state is attained at $\varepsilon=40-50\%$. The value and extension of the stress peak are dependent (albeit non-significantly) on the deformation temperature, and are mainly determined by the strain rate.

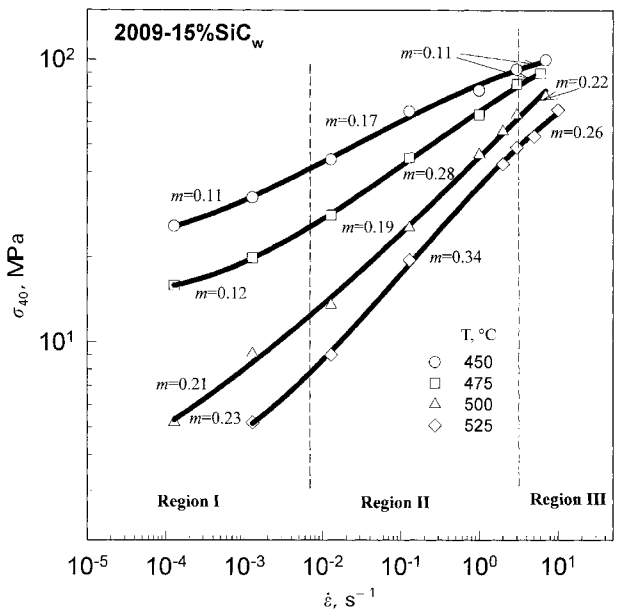

2 Strain rate dependence of flow stress at given temperatures: coefficient of strain rate sensitivity m has been calculated in accordance with equation (2)

Strain rate–steady state stress dependence

The strain rate versus steady state stress dependence is described by the power law given in equation (1) (Fig. 2). Inspection shows that there is evidence for a sigmoidal relationship between the flow stress and the strain rate, plotted on a double logarithmic scale, over the entire temperature interval under study. Three classic strain rate regions of superplasticity[4,5] can be distinguished (Fig. 2). In the temperature interval 450–475°C, the value of m in region II is larger than in regions I and III by a factor of ~1·5, but is significantly less than a typical value of m for superplasticity.[5] Increasing the temperature leads to an increase of coefficient m in region II from $m=0{\cdot}17$ at $T=450$°C to $m=0{\cdot}34$ at $T=525$°C, in the strain rate interval $1{\cdot}2\times10^{-2}-2\times10^{0}$ s^{-1}. Notably, the σ–ε curves exhibiting steady state flow occur in region I, and the other type of curve can be observed to occur in regions II and III.

The above σ–ε dependencies are typical for manifestation of the superplastic effect,[5] and are very similar to those for the present composite found by tension testing.[12,13] The transition from tensile deformation to compression results in a shift of the optimal strain rate interval for superplastic flow towards higher strain rates by one order of magnitude, as found in bulk materials.

SHAPE OF COMPRESSED SPECIMENS

The anisotropy of plastic flow of the 2009Al–15%SiC$_w$ composite yields non-uniform compression. The anisotropic shape can be determined as a ratio of the major axis of the ellipse a to the minor axis b (Fig. 3). With increasing strain rates, aspect ratio a/b values decrease gradually in region I, while in region II they decrease rapidly and attain unity in region III (Fig. 3). Therefore, the increase in strain rate causes the plastic flow to be more uniform and, as a result, the compressed specimens become circular in cross-section. Similar results were reported in the work of Gonzalez-Doncel *et al.*,[17] and were attributed to the initial whisker distribution.

It can be expected that the anisotropic plastic flow is associated with the initial crystallographic texture. However, X-ray analysis showed that the initial texture of the matrix was relatively weak, and no discernible texture changes were revealed after plastic deformation in the first

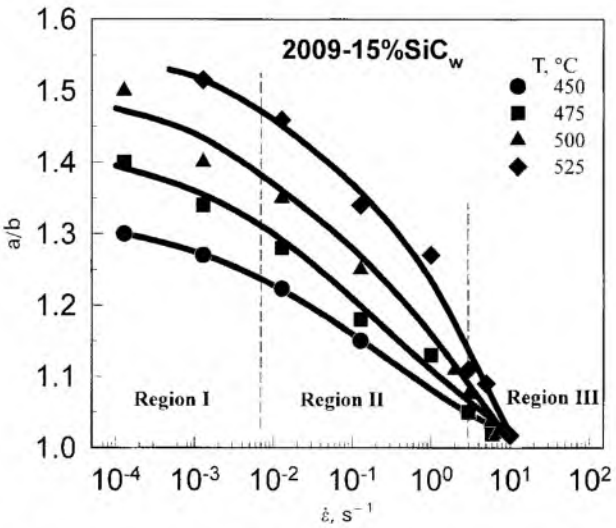

3 Aspect ratio a/b as function of strain rate at given temperatures

and second regions. Therefore, the initial texture is not important for uniformity of plastic deformation in the composite.

INITIAL MICROSTRUCTURE

The initial microstructure of the as processed 2009Al – 15%SiC_w billet is shown in Figs. 4 and 5. It can be seen that the majority of reinforcing elements are 4 μm in length and ~0·5 μm in diameter. They are aligned along the initial rolling direction. The distribution of the SiC_w within the aluminium matrix is not entirely uniform. Two structural components can be distinguished in the as received material, in both longitudinal and transverse sections. The first structural component, defined as the whisker containing area (WCA), prevails. The second structural component occupies ~20% of the entire material volume, and is defined as the whisker free area (WFA). Furthermore, irregular WFAs are elongated along the rolling direction.

The average matrix grain size of the as received composite is 3 μm. The grain structure of the composite matrix is generally non-uniform. There are relatively large grains elongated along the former rolling direction (5 – 10 μm in the longitudinal direction and 2 – 5 μm in the transverse

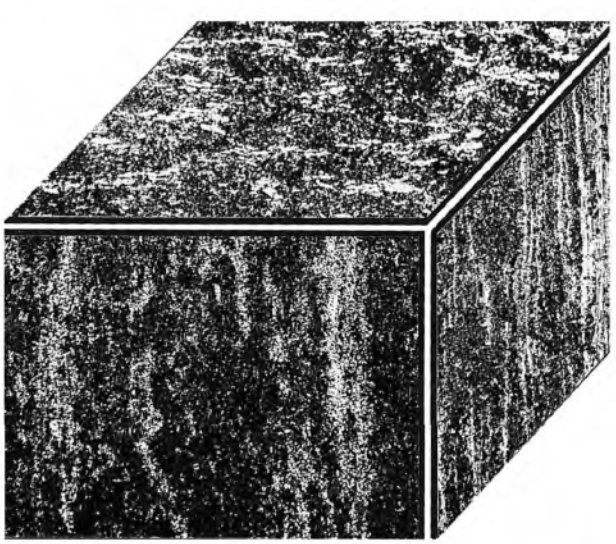

4 Three-dimensional grain microstructure of as received 2009Al – 15%SiC_w composite

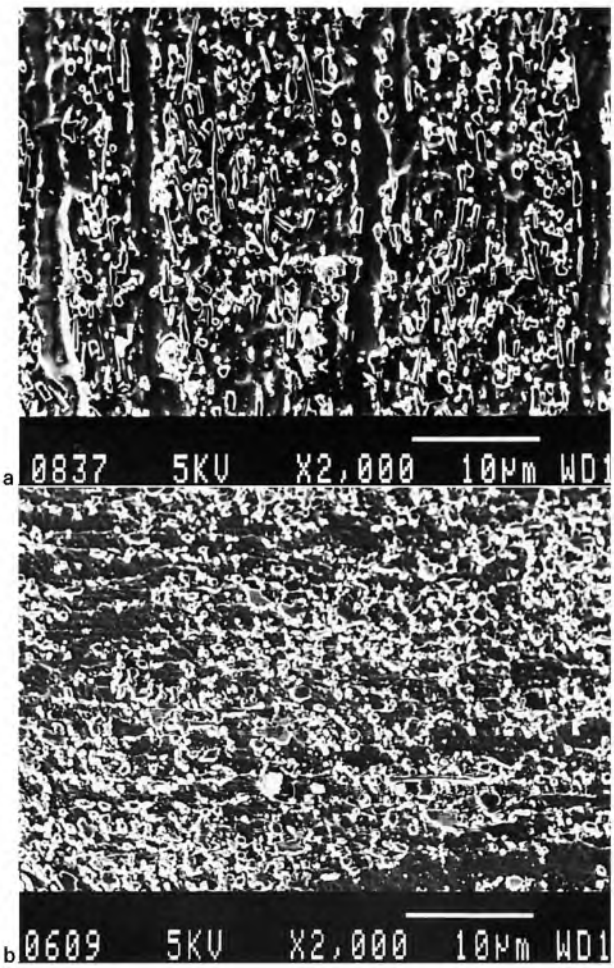

a parallel to compression axis; *b* perpendicular to compression axis

5 Microstructure of compression specimen of 2009Al–15%SiC_w composite in given sections

direction) in WFAs. Finer grains with a size of less than 3 μm are present in WCAs. A high grain aspect ratio was determined by TEM. The average lattice dislocation density is not high ($\rho = 1{\cdot}5 \times 10^{13}$ m^{-2}) (*see* Fig. 6)

STRUCTURAL EVOLUTION

Macrostructure at level of specimen

The macrostructure that evolved in the 2009Al – 15%SiC_w composite was found to be strain rate dependent (Fig. 7). In region I, the formation of symmetrical type of macrostructure takes place (Fig. 7*a*). Plastic flow lines (PFLs) are revealed by chemical etching. As the temperature or strain rate increases, the plastic flow becomes more homogeneous. In region II, no significant changes in the macrostructure occur under deformation (Fig. 7*b*). In region III, a further strain rate increase ($\dot{\varepsilon} \geqslant 1$ s^{-1}) results in the disappearance of the previous macrostructure and the formation of a new, non-symmetrical structure. As can be seen from Fig. 7*c*, the PFLs are clearly rearranged at an angle of ~45° to the compression axis. At $T = 525$°C in region III, the evolved macrostructure has a strong orientation towards plastic flow (Fig. 7*d*).

Microstructure at level of grain groups

Plastic deformation in region I leads to randomisation of the SiC_w distribution in the central part of the specimen cross section (Fig. 8). The whiskers have a tendency to

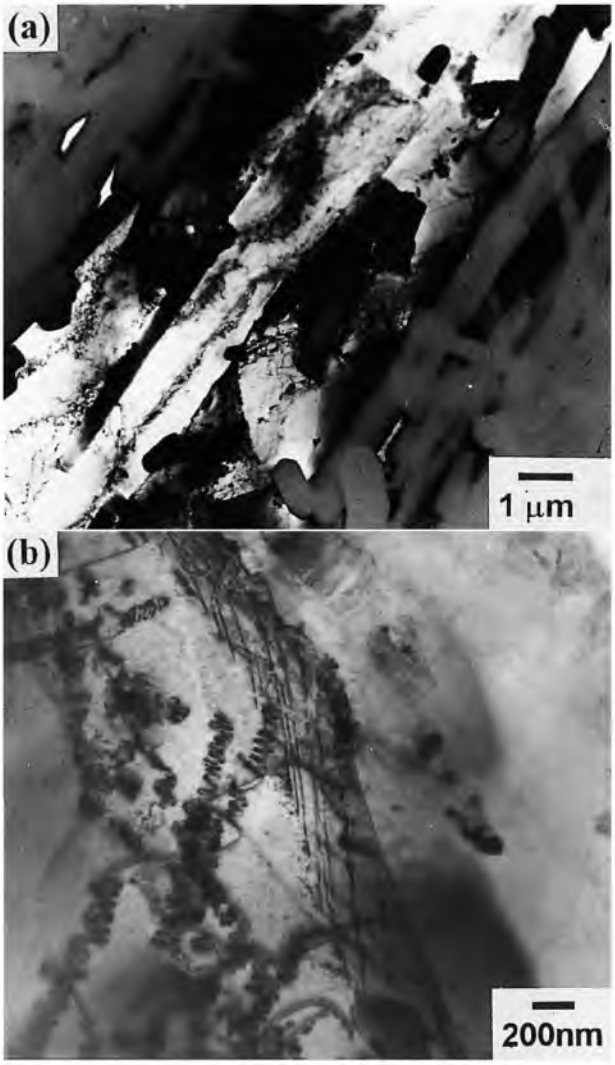

a longitudinal section showing alumina dispersoid aligned along grain boundaries; *b* extrinsic grain boundary dislocations formed during cooling

6 Images (TEM) of the as received 2009Al–15%SiC_w composite

rotate towards plastic flow. As a result, the SiC whiskers align along the PFLs. Notably, the matrix grains of separated WFAs elongate in the direction of the major axis of the specimen ellipse (Fig. 8*a*). An increase in temperature provides increased structural uniformity.

In region II, most of the whiskers retain their initial orientation. A minority of SiC_w are rearranged along direction *b* (Fig. 8*b*). Matrix grains in WFAs attain an equiaxed shape. Most of the WFAs are bent, and elongated towards plastic flow.

There is a strong temperature dependence of microstructure formation in region III. A great number of reinforcements are strongly aligned along the PFLs, which are close to 45° to the compression axis (Fig. 8*c*). A temperature increase leads to a slight randomisation of their distribution (Fig. 8*d*). Matrix grains are elongated towards the PFLs. Plastic deformation results in elongation of the WFAs along the PFLs, and their subsequent disruption.

The effect of strain rate on the size and shape of the matrix grains is summarised in Table 1. In general, the plastic deformation provides a more equiaxed shape of the matrix grains, in comparison with the initial state of the composite. In region II, equiaxed grains with an average size of 3–4 μm are evolved, while in region I elongated grains are observed. Their aspect ratio decreases as the temperature increases. In contrast, a random grain size distribution is observed in region III at high temperatures. The size of small grains is ~1 μm, whereas the size of coarse grains is ~6 μm. It can be concluded that dynamic recrystallisation occurs in region III.

Microstructure at level of grain

Observations by TEM suggest that different dislocation structures form in the three strain rate regions. Homogeneously distributed dislocations with a density of $\sim 5 \times 10^{13}$ m^{-2} are found after deformation in region I (Fig. 9*a*). Most of the dislocations belong to one glide system.[14] Dislocation pileups are observed near Al/SiC_w interfaces.

The average dislocation density decreases slightly to $\rho = 7 \times 10^{12}$ m^{-2} during superplastic deformation in region II. In WFAs the elongated grains exhibit a higher dislocation density, while within the equiaxed grains the lattice dislocations are rarely observed (Fig. 9*b*). Examination of the microstructure by TEM indicates that dislocation walls stabilised by dispersoid particles are formed inside some of the matrix grains. The small grains with a comparatively high density of dislocations are located in several WCAs (Fig. 9*c*). The influence of temperature on the fine structure in region II is negligible.

In region III, the formation of subgrains with a size of ~2 μm is observed in WFAs (Fig. 9*d*). The dislocation density within the subgrain is found to be $1{\cdot}2 \times 10^{12}$ m^{-2} at $T = 525$°C. In WCAs, tangled dislocations are revealed ($\rho = 2. \times 10^{13}$ m^{-2}). This dislocation structure is typical of multiple dislocation glide.[18]

Fine precipitates (15–20 nm) effectively pin lattice dislocations in the vicinity of the boundaries Al/Al and Al/SiC_w (Fig. 10*a*) at $T = 525$°C. At the same time, it is found that grain boundaries Al/Al are almost free from dispersoids at $T \leqslant 500$°C. Perhaps an oxide forms on the grain boundaries at $T = 525$°C.[13]

The important feature of the strained structure of the composite is that of well defined grain boundary dislocations (Fig. 10*b*). The density of grain boundary dislocations increases strongly with decreasing deformation temperature. This testifies that the process of dislocation absorption by grain boundaries in the 2009Al–15%SiC_w composite occurs slowly and only at temperatures close to the melting temperature.[16]

Thus, the previous orientation of the SiC_w is retained during deformation in region II. Superplastic deformation results in decreased lattice dislocation density. In regions I and III, extensive rotation of the whiskers takes place, leading to loss of directionality in the reinforcements. This process is associated with increasing lattice dislocation density.

Surface observations

Surface observations of deformed specimens shown in Fig. 11 demonstrate that sliding along intergranular boundaries is the main contributor to total elongation under optimal superplastic conditions. Offset of scratch marks is

Table 1 Influence of temperature and strain rate on average grain size (μm): ε=50%

	Strain rate, s^{-1}		
Temperature, °C	$1{\cdot}28 \times 10^{-4}$	$1{\cdot}28 \times 10^{-1}$	1×10^{0}
450	2·5/5*	3·8	2·5
500	3·6	3·5	4
525	2·9/4·5*	3·3	2·9/5*

*Size in transverse direction/size in longitudinal direction of whisker free areas.

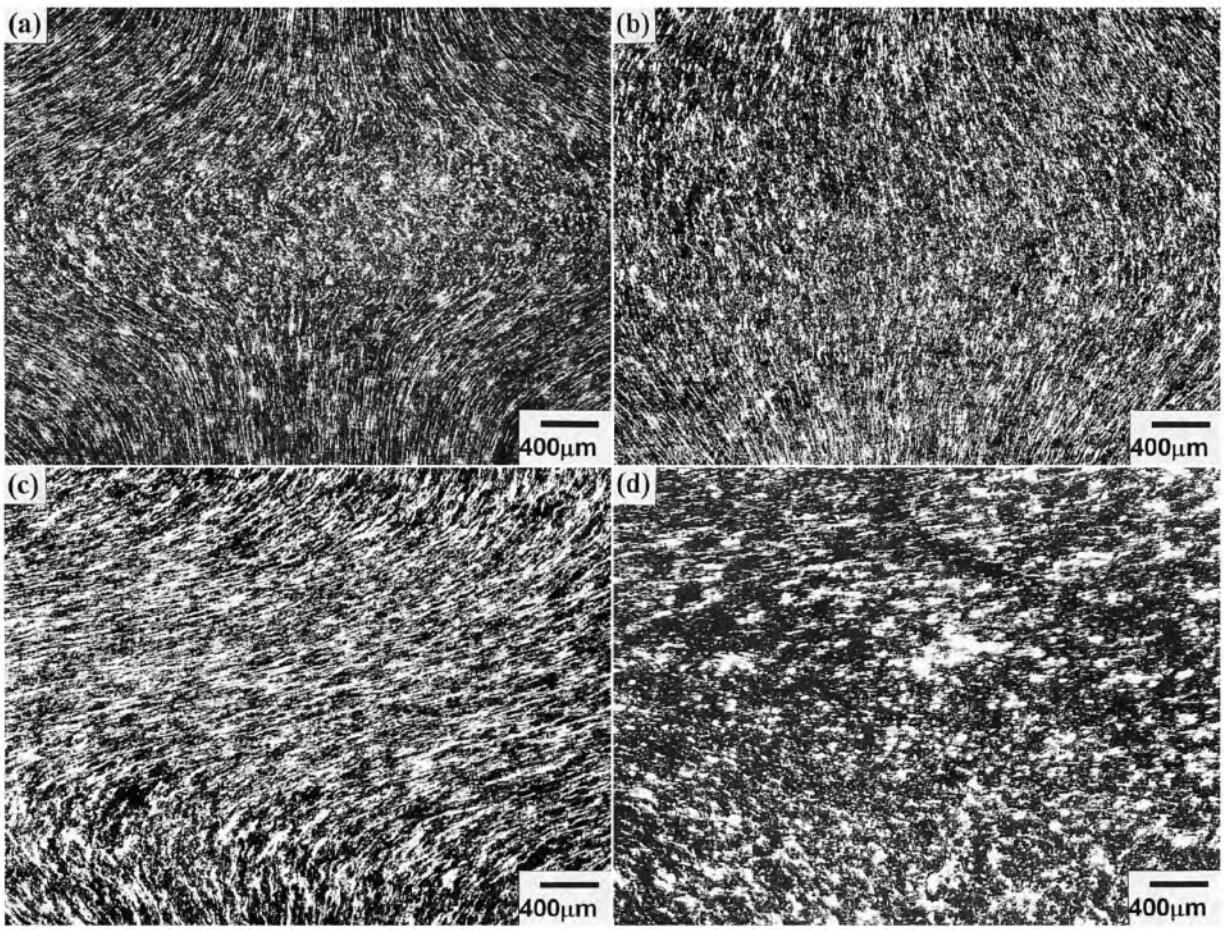

a $T=450°C$, $\dot{\varepsilon}=1{\cdot}3\times10^{-4}\ s^{-1}$; *b* $T=500°C$, $\dot{\varepsilon}=1{\cdot}3\times10^{-1}\ s^{-1}$; *c* $T=450°C$, $\dot{\varepsilon}=6\ s^{-1}$; *d* $T=525°C$, $\dot{\varepsilon}=1\times10^{1}\ s^{-1}$

7 Macrostructures of 2009Al–15%SiC_w composite after deformation under given conditions: cross-sections

not observed along Al/SiC_w interfacial boundaries. At the same time, there is evidence for extensive sliding along intergranular boundaries (Fig. 11*a*), occurring mainly in a cooperative manner[19,20] (Fig. 11*b*). Similar to what is seen in bulk materials,[19,20] localised deformation bands oriented at an angle of 30–60° to the compression axis are observed (Fig. 11*b*). The appearance of these bands is caused by a shift of matrix grain groups as a unit along common grain boundary surfaces.[19,20] It is known[19,20] that the formation of continuous stringers of cooperative grain boundary sliding (CGBS) is a necessary condition for superplasticity. Unlike in monolithic alloys, propagation of these bands in the present material is retarded by the whiskers. As a result, bands of CGBS propagate around the SiC_w (Fig. 11*b*), which highly increases the uniformity of the grain boundary sliding. Spacing between the CGBS surfaces in the composite is less than in bulk alloys[19] by a factor of ~4, and approaching the size of the matrix grains with increasing strain. This seems to be the main reason for a shift of the optimal superplastic strain rate towards higher values.

Heterogeneous grain boundary sliding is found at lower strain rates in the present work. In region I, the CGBS along one direction dominates strongly (Fig. 11*c*). The WFAs can play the role of grain groups shifting as a unit.

SERVICE PROPERTIES

To evaluate the effect of superplastic deformation, the service mechanical properties of 2009–15%SiC_w composite were examined in the as received condition and after HSRS (Table 2). It is clearly seen that HSRS exerts a positive effect on service properties of the 2009–15%SiC_w composite by increasing tensile strength and toughness.

Analysis of results and discussion

The above results lead to the conclusion that characteristics of microstructural evolution in 2009Al–15%SiC_w composite during superplastic deformation are associated with features of grain boundary sliding in this material. To provide evidence for this, a detailed analysis of superplastic behaviour is given below.

Table 2 Ambient temperature mechanical properties of 2009Al–15%SiC_w composite: T6 condition

Condition*	Tensile strength, MPa	0·2% yield strength, MPa	Elongation, %	Fracture strength, MPa	Fracture toughness K_{CU}, kJ m^{-2}
As received	650	490	5	800	200
After SPD	675	495	6	900	275

*SPD is superplastic deformation: $T=500°C$, $\dot{\varepsilon}=5\times10^{-2}\ s^{-1}$, $\varepsilon=70\%$.

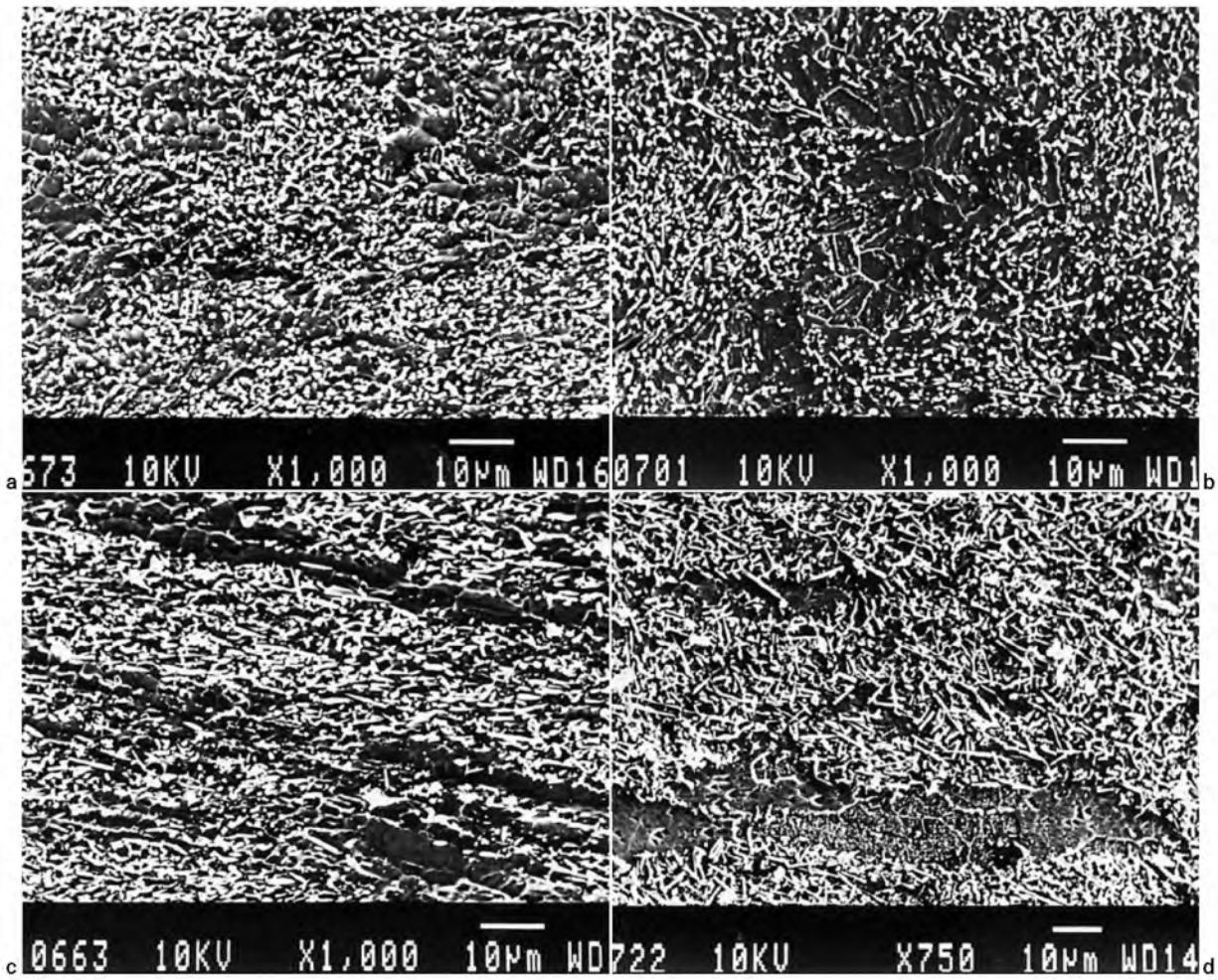

a $T=450°C$, $\dot{\varepsilon}=1{\cdot}3\times10^{-4}$ s^{-1}; *b* $T=500°C$, $\dot{\varepsilon}=1{\cdot}3\times10^{-1}$ s^{-1}; *c* $T=450°C$, $\dot{\varepsilon}=6\times10^{0}$ s^{-1}; *d* $T=525°C$, $\dot{\varepsilon}=1\times10^{1}$ s^{-1}

8 Microstructures of 2009Al–15%SiC$_w$ composite deformed under given conditions

SUPERPLASTIC BEHAVIOUR

Threshold stress

It is known[21] that the most important feature of the deformation behaviour of MMCs produced via powder metallurgy is the presence of a threshold stress. In this case, equation (1) may be represented by[21–23]

$$\dot{\varepsilon}=A\left(\frac{\sigma-\sigma_{th}}{G}\right)^{n}\exp\left(-\frac{Q_c}{RT}\right) \quad . \quad . \quad . \quad . \quad . \quad . \quad . \quad (3)$$

where σ is the applied stress, σ_{th} is the threshold stress, G is the shear modulus, n is the true stress exponent, Q_c is the true activation energy, and T is the absolute temperature.

Values of the threshold stress σ_0 can be estimated by plotting $\dot{\varepsilon}^{1/n}$ against σ on a double linear scale for selected values of n.[21] This graphical method can be used if the deformation of the composite obeys dependence according to equation (3), and if σ_{th} is constant for each test temperature and independent of the strain rate.[21] Previous estimations have shown that these circumstances hold in regions I and II.[24] The data points from these strain rate intervals fit with excellent accuracy to a straight line whose extrapolation to zero gives the value σ_{th}. The present consideration is restricted to these data. At highest strain rates, i.e. $\varepsilon\geqslant10^{0}$ s^{-1}, the values of σ_{th} are different.

Figure 12 shows a plot of $\dot{\varepsilon}^{1/n}$ versus σ for $n=3$. The stress exponent of 3 yields the best linear fit between $\dot{\varepsilon}^{1/n}$ and σ for all temperatures examined. Thus, values of σ_{th} at 450, 475, 500, and 525°C are estimated to be 2, 4, 13, and 22·5 MPa, respectively. The temperature dependence of the normalised threshold stress σ_{th}/G is presented in Fig. 13. It is clearly seen that σ_{th} decreases linearly with increasing temperature. This temperature dependence obeys[21–24]

$$\frac{\sigma_{th}}{G}=B_0\exp\left(\frac{Q_0}{RT}\right) \quad . \quad . \quad . \quad . \quad . \quad . \quad . \quad . \quad . \quad . \quad . \quad (4)$$

where B_0 is a constant and Q_0 is an energy term.

The value $Q_0=160$ kJ mol^{-1} can be obtained graphically by plotting $\ln\sigma_{th}/G$ versus $1/T$. It is interesting to note that this type of dependence was observed in classic superplastic materials.[24] It has been suggested[25,26] that an interaction between grain boundary dislocations and impurity atoms segregated at grain boundaries should give rise to a threshold stress dependence as given in equation (3). In this case, Q_0 represents the binding energy between an impurity atom and a dislocation.[25] The Q_0 value obtained is greater than the values near 25 kJ mol^{-1} reported for superplastic materials produced by ingot metallurgy,[25] and corresponds with Q_0 values observed for several superplastic composites produced by the the powder metallurgy technique.[25]

It seems that in the 2009Al–15%SiC$_w$ composite, oxygen is an impurity atom responsible for the above high value of the energy term. It has been indicated[26] that during powder metallurgical processing some amount of oxygen is introduced into the aluminium matrix. As a result, the formation of uniformly distributed nanoscale oxide particles can occur.[21,25–27] It appears that interstitial oxygen concentrates in segregation at Al/Al boundaries at $T\leqslant500°C$, and forms dispersoids at $T\geqslant525°C$.

Thus, analysis of superplastic behaviour shows that there exists strong binding energy between a grain boundary dislocation and impurity atoms[24,24,27] resulting in dramatic

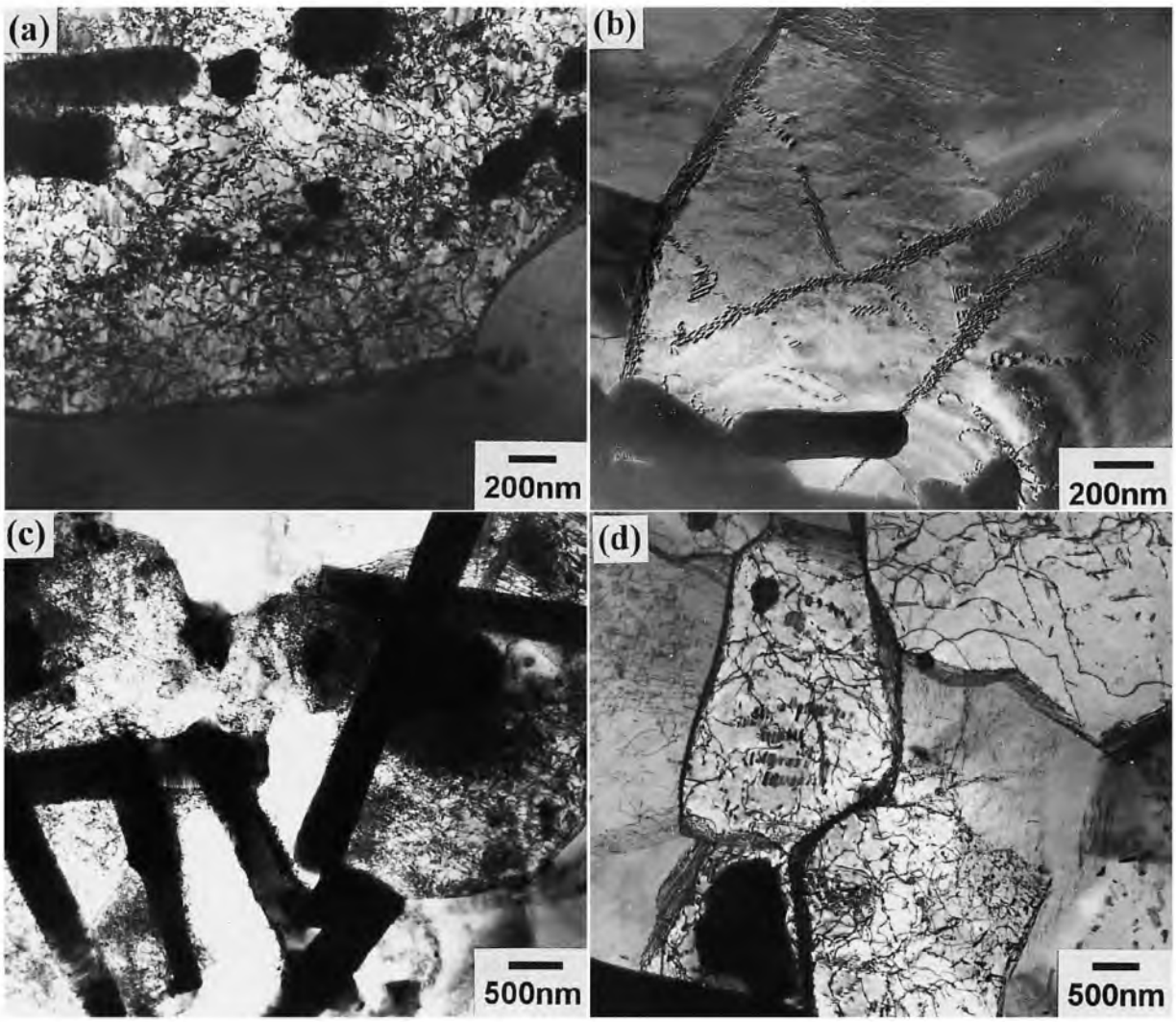

a $T=450°C$, $\dot{\varepsilon}=1{\cdot}3\times10^{-4}$ s^{-1}; *b* $T=525°C$, $\dot{\varepsilon}=1{\cdot}3\times10^{-1}$ s^{-1}; *c* $T=450°C$, $\dot{\varepsilon}=6\times10^{0}$ s^{-1}; *d* $T=525°C$, $\dot{\varepsilon}=1\times10^{1}$ s^{-1}

9 Images (TEM) of 2009Al–15%SiC_w composite after deformation under given conditions

increase in temperature of absorption of dislocations by grain boundaries.[16] This is why grain boundary dislocations can be observed after superplastic deformation. Enhanced flow stress becomes necessary for grain boundary sliding. As a result, the optimal interval of superplasticity shifts towards a higher strain rate.

Activation energy

The true activation energy of deformation was computed assuming that equation (2) adequately describes the deformation behaviour of the composite. Hence, Q_c was determined according to[21]

$$Q_c = -R\left.\frac{\partial(\log\dot{\varepsilon})}{\partial(1/T)}\right|_{\sigma-\sigma_{th}} \quad \ldots\ldots\ldots\ldots \quad (5)$$

Figure 14 shows the $\ln\dot{\varepsilon}$ versus $1/T$ dependencies for three different $\sigma-\sigma_{th}$ levels. The calculated activation energy in each region of effective stress is slightly higher than the activation energy for lattice self-diffusion (142 kJ mol^{-1}).

Examination of normalised deformation data

Figure 15 shows a double logarithmic plot of the normalised strain rate $\dot{\varepsilon}kT/D_L Gb$, where k is the Boltzmann constant, D_L is the lattice diffusion coefficient, and b is the Burgers vector, versus the normalised effective stress $(\sigma-\sigma_{th})/G$. The standard dependencies of the lattice diffusion coefficient and shear modulus on temperature for bulk aluminium[25–27] were used. It is known that there is no significant change in the temperature dependence of the shear modulus of the matrix as a result of the presence of reinforcing elements.[25–27] It is demonstrated that, in the temperature–strain rate interval studied, there is a well defined power law relationship with $n=3$, representing a least squares fit to the data points.

OPERATING DEFORMATION MECHANISMS AND MICROSTRUCTURAL EVOLUTION

The values of the true stress exponent and the true activation energy indicate that the rate controlling process of superplastic deformation in the composite is associated with the glide of lattice dislocations.[4,21] At the same time, the results of structural investigation give evidence for the operation of grain boundary sliding along intergranular boundaries. This process plays an important role in microstructural evolution and uniformity of plastic deformation. Grain boundary sliding accelerates the dissociation of lattice dislocations trapped by grain boundaries,[16] which begin to play the role of sinks for mobile lattice dislocations.[5]

It is known[28,29] that the formation of distorted regions in the vicinity of SiC whiskers, owing to local dislocation accumulation, leads to their rotation during deformation.

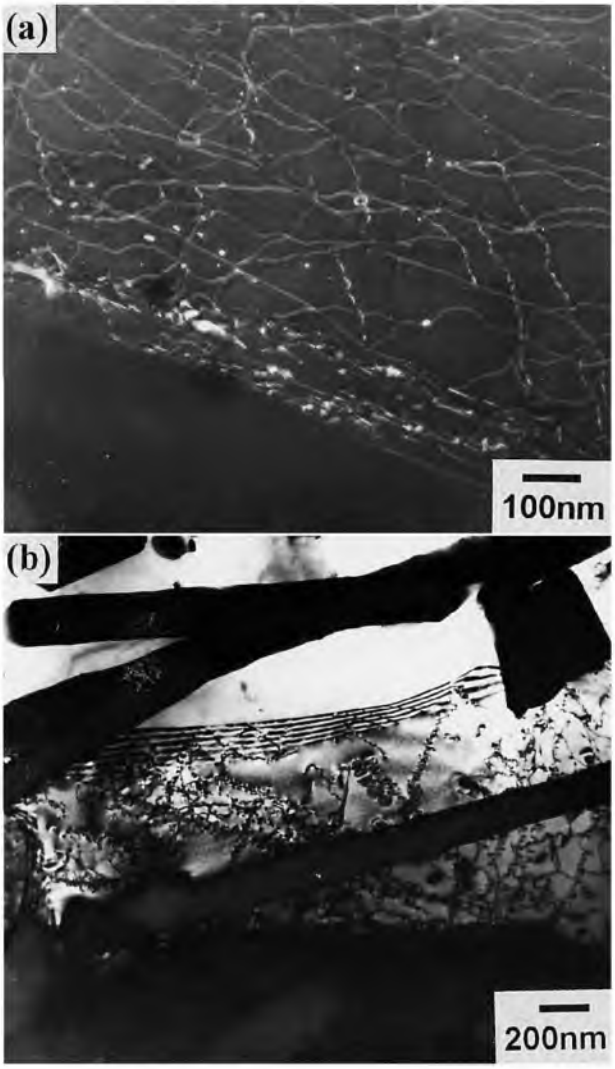

a dark field mode (for reflection 220) showing interaction of extrinsic lattice dislocations with precipitates located at grain boundaries; *b* showing absorption of lattice dislocations into grain boundaries

10 Images (TEM) of 2009Al–15%SiC_w composite after deformation at 525°C and $\dot{\varepsilon}=1{\cdot}3\times10^{-1}$ s^{-1}

In region II, extensive and uniform grain boundary sliding yields decreased dislocation density. As a result, the whisker rotations are negligible (Fig. 16*b*), since no remarkable accumulation of lattice dislocations takes place near SiC_w/Al boundaries. Uniformity of plastic flow and keeping the initial directionality of the reinforcements during superplastic deformation is associated with homogeneous grain boundary sliding (Fig. 16*b*). Strain softening during superplastic deformation is caused by decreasing lattice dislocation density and increasing uniformity of grain boundary sliding with strain increase.

In regions I and III, the contribution of grain boundary sliding to total deformation is essentially less. In region I, grain boundary sliding occurs non-uniformly along several boundary surfaces, and in region III, multiple slip makes the main contribution to total deformation. As a result, the grain boundaries do not have the ability to adsorb all the mobile lattice dislocations which accumulate within the grains. Extensive rotation of the reinforcements and their alignment towards plastic flow takes place (Fig. 16*a* and *c*). In region I, a combination of heterogeneous grain boundary sliding and single dislocation slip leads to easier plastic flow along the initial orientation of the SiC whiskers and WFAs (Fig. 16*a*). High anisotropy of

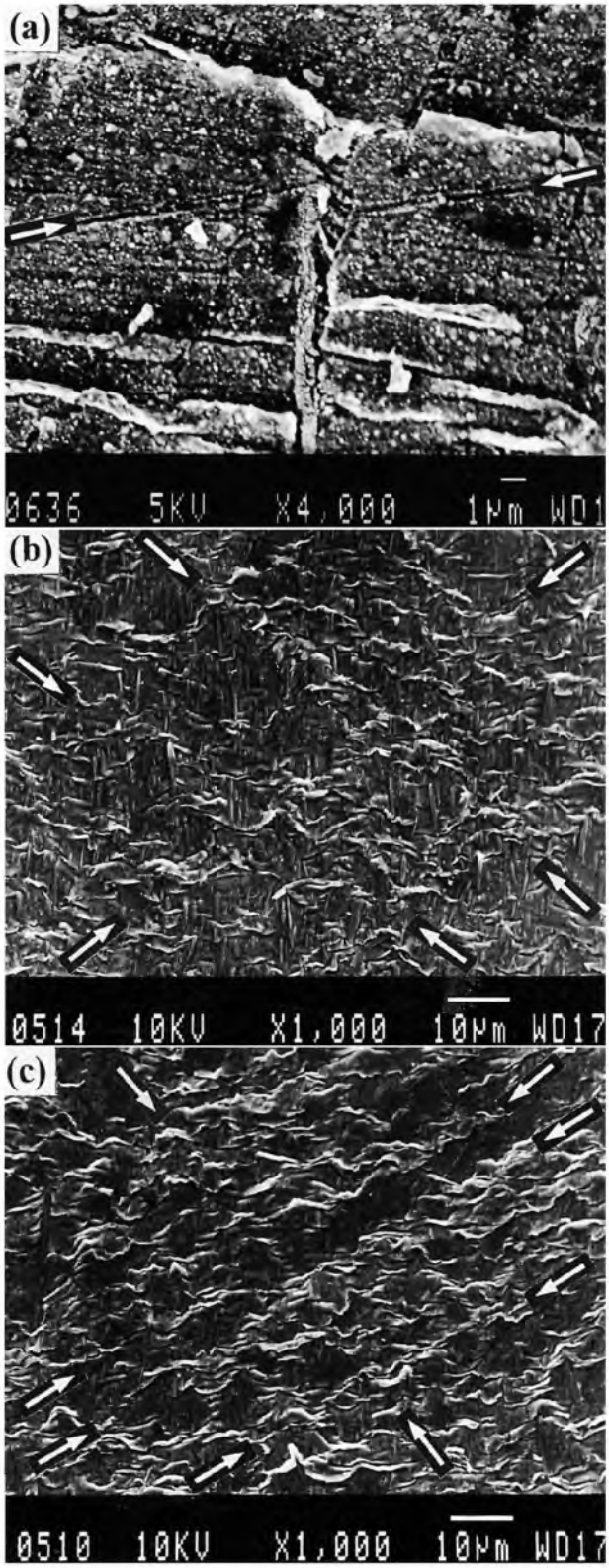

a $\dot{\varepsilon}=1{\cdot}3\times10^{-1}$ s^{-1}, $\varepsilon=12\%$; *b* $\dot{\varepsilon}=1{\cdot}3\times10^{-1}$ s^{-1}, $\varepsilon=25\%$; *c* $\dot{\varepsilon}=1{\cdot}3\times10^{-3}$ s^{-1}, $\varepsilon=25\%$

11 Surface observations of 2009Al–15%SiC_w composite after deformation at 525°C and given strains and strain rates

plastic deformation on a macroscopic level takes place. In region III, multiple slip is accompanied by uniform grain boundary sliding (Fig. 16*c*), and plastic deformation occurs uniformly.

In region I, the establishment of steady state flow results from the occurrence of CGBS along surfaces of easiest

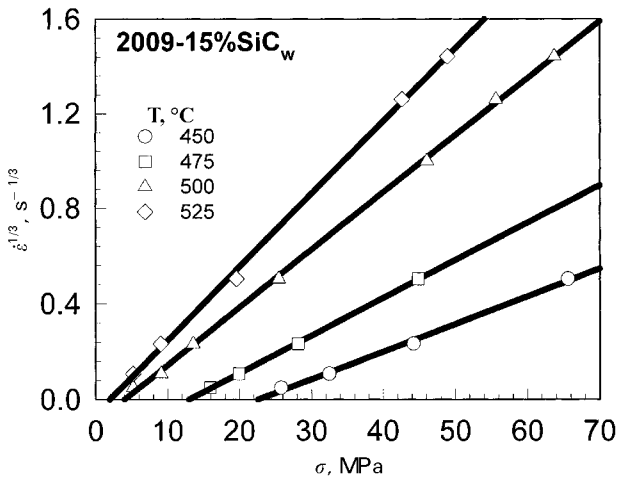

12 Plot of $\dot{\varepsilon}^{1/n}$ *v.* σ for 2009Al–15%SiC_w composite at given temperatures for $n=3$

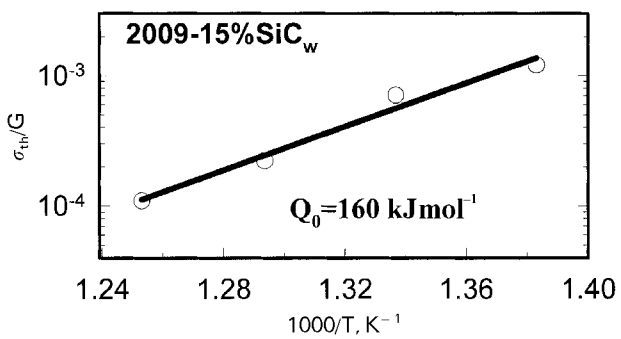

13 Plot of logarithm of normalised threshold stress σ_{th}/G *v.* $1/T$ for 2009Al–15%SiC_w composite

sliding. At higher strain rates, a transition from CGBS to uniform grain boundary sliding leads to the establishment of a steady state.

Thus, superplastic deformation is a unique fabrication route that retains the initial directionality of the reinforcements. This is a result of the features of the operating deformation mechanism. An enhancement of service properties can be attained by the use of superplastic deformation.

Conclusions

1. The composite 2009Al–15%SiC_w, examined in compression at $T=450-525$°C and $\dot{\varepsilon}=10^{-4}-10^{1}$ s^{-1}, exhibits a superplastic like behaviour at $T=500-525$°C in the strain rate interval $10^{-2}-10^{0}$ s^{-1}, which is one order of magnitude higher than that in tension.

2. The superplastic behaviour of the composite has been considered in terms of a threshold stress. The stress exponent n has the value 3 and the true activation energy for plastic deformation is ~148 kJ mol^{-1}. A strong dependence of threshold stress versus temperature with the energy term $Q_0=160$ kJ mol^{-1} has been found.

3. Sliding along intergranular boundaries within the aluminium matrix occurs during superplastic deformation. No evidence has been found for interfacial sliding. The SiC whiskers provide high uniformity of grain boundary sliding.

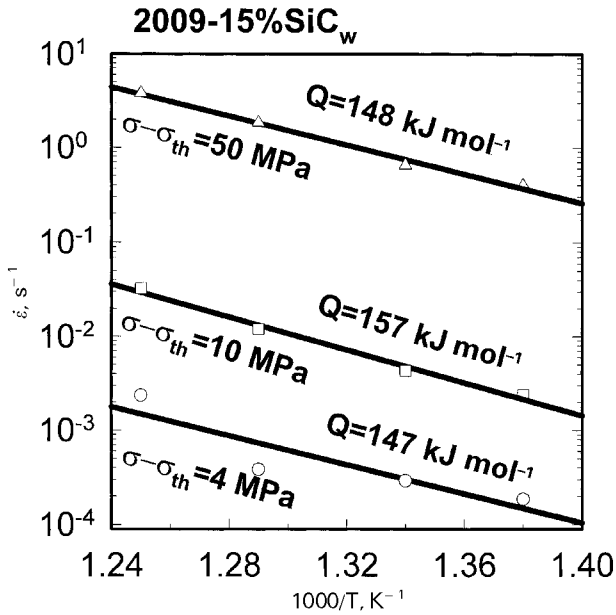

14 Strain rate log$\dot{\varepsilon}$ as function of temperature $1/T$ at given effective stresses $\sigma-\sigma_{th}$

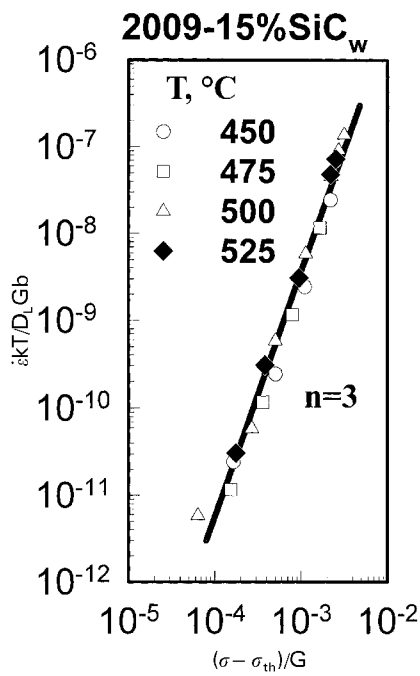

15 Double logarithmic plot of normalised strain rate versus normalised effective stress is regions I and II for 2009Al–15%SiC_w composite

4. The shape of compressed specimens and orientation of SiC_w depend strongly on strain rate. The SiC whiskers retain their directionality during superplastic deformation. The reinforcements rotate and align towards plastic flow during deformation at both lower and higher strain rates. In region I, a strong anisotropy of plastic flow at macroscopic level takes place.

5. It has been found that superplastic deformation results in decreased lattice dislocation density. Deformation at lower or higher strain rates leads to increased dislocation density. In region III, dynamic recrystallisation occurs in coarse matrix grains. Enhanced dislocation density is observed near SiC/Al boundaries.

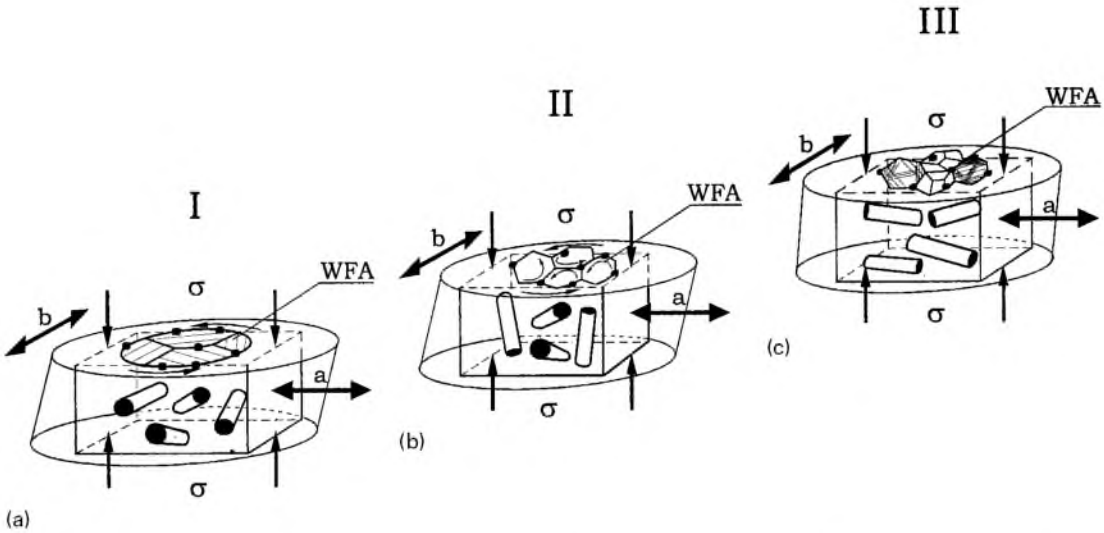

a I; *b* II; *c* III

16 Schematic representation of realignment of whiskers and deformation mechanism in whisker free areas (WFAs) during hot compression deformation in given regions: *a* and *b* are axes of ellipse, *a* direction of maximum deformation

References

1. E. A. STARKE, T. H. SANDERS, and I. G. PALMER: *J. Met.*, 1981, **33**, 24–33.
2. F. H. FROES and J. P. PICKENS: *J. Met.*, 1984, **36**, 14–28.
3. T. G. NIEH and J. WADSWORTH: *Mater. Sci. Eng. A*, 1991, **A147**, 129–142.
4. T. G. NIEH, J. WADSWORTH, and O. D. SHERBY: 'Superplasticity in metals and ceramics', 210; 1996, New York, Cambridge University Press.
5. O. A. KAIBYSHEV: 'Superplasticity of alloys, intermetallides, and ceramics', 316; 1992, Berlin, Springer-Verlag.
6. M. G. MCKIMPSON and T. E. SCOTT: *Mater. Sci. Eng. A*, 1989, **A107**, 93.
7. Y. L. LIU, N. HANSEN, and D. J. JENSEN: *Mater. Sci. Technol.*, 1991, **7**, 270–275.
8. H. Y. KIM and S. H. HONG: *Scr. Metall. Mater.*, 1994, **30**, 297–302.
9. D. G.-C. SYU and A. K. GHOSH: *Metall. Trans. A*, 1994, **25A**, 2049–2061.
10. J. R. PICKENS, T. J. LANGAN, R. O. ENGLAND, and M. LIEBSON: *Metall. Trans. A*, 1987, **18A**, 303.
11. R. KAIBYSHEV, V. KAZYHANOV, and J. STOBRAWA: *Phys. Met. Metallogr.*, 1996, **2**, 133–144.
12. C. C. BAMPTON, R. KAIBYSHEV, and V. KAZYKHANOV: *Mater. Sci. Forum*, 1997, **243–245**, 161–167.
13. R. S. MISHRA, C. ECHER, C. C. BAMPTON, T. R. BIELER, and A. K. MUKHERJEE: *Scr. Mater.*, 1996, **35**, 247–252.
14. YU. M. VAINBLAT (ed.): 'Methods of control and examination of light alloys', 510; 1985, Moscow, Metallurgia (in Russian).
15. P. B. HIRSH, A. HOWIE, R. B. NICHOLSON, D. W. PASHLEY, and M. J. WHELAN: 'Electron microscopy of thin crystals', 574; 1965, London, Butterworths.
16. O. KAIBYSHEV and R. VALIEV: 'Grain boundaries and properties of metals', 213; 1987, Moscow, Metallurgia (in Russian).
17. G. GONZALEZ-DONCEL, S. D. KARMARKAR, A. P. DIVECHA, and O. D. SHERBY: *Compos. Sci. Technol.*, 1989, **35**, 105–120.
18. F. LI, W. T. ROBERTS, and P. S. BATE: *Acta Mater.*, 1996, **44**, 217.
19. M. G. ZELIN, N. A. KRASILNIKOV, R. Z. VALIEV, M. W. GRABSKI, H. S. YANG, and A. K. MUKHERJEE: *Acta Metall. Mater.*, 1994, **42**, 119–126.
20. V. V. ASTANIN, O. A. KAIBYSHEV, and S. N. FAIZOVA: *Acta. Metall. Mater.*, 1994, **42**, 2617–2622.
21. F. A. MOHAMED, K. T. PARK, and E. J. LAVERNIA: *Mater. Sci. Eng. A*, 1992, **A150**, 21–35.
22. G. GONZALEZ-DONCEL and O. D. SHERBY: *Acta Metall. Mater.*, 1993, **41**, 2797–2805.
23. R. S. MISHRA, T. R. BIELER, and A. K. MUKHERJEE: *Acta Mater.*, 1997, **45**, 561–568.
24. S. YAN, C. EARTHMAN, and F. MOHAMED: *Philos. Mag. A*, 1994, **69**, 1017–1038.
25. K. T. PARK, E. LAVERNIA, and F. MOHAMED: *Acta Metall. Mater.*, 1994, **42**, 667–678.
26. K. T. PARK, E. LAVERNIA, and F. MOHAMED: *Acta Metall.*, 1990, **38**, 2149–2154.
27. Y. LI, S. R. NUTT, and F. MOHAMED: *Acta Mater.*, 1997, **45**, 2607–2619.
28. F. J. HUMPHREYS, W. S. MILLER, and M. R. DJAZEB: *Mater. Sci. Technol.*, 1990, **6**, 1157–1169.
29. C. Y. BARLOW and N. HANSEN: *Acta Metall. Mater.*, 1991, **39**, 1971–1979.